Original Research Paper

Investigating Sintering Mechanisms for Additive Manufacturing of Conductive Traces

Jasmine McKenzie and Salil Desai

Department of Industrial and Systems Engineering,
North Carolina A and T State University, Greensboro, USA

Abstract: Additive Manufacturing (AM) processes enable the fabrication of miniaturized and flexible devices on complex geometries. This paper explores a hybrid additive manufacturing technology that integrates micro-extrusion and PICO-jetting methods. Conductive slurries and colloidal inks were optimized for their rheological properties to aid their precise deposition. A variety of conductive materials which include carbon, silver, nano-particle silver and nickel were deposited on both rigid (glass) and flexible (Kapton) substrates. The deposited traces were cured using two sintering mechanisms which include furnace heating and in situ laser irradiation. The effect of curing mechanism on the conductance of deposited traces was evaluated. The results indicated that traces could be cured successfully with the laser curing mechanism. Nickel and silver laser cured traces had lower resistivity than the furnace sintered traces. An increase in the laser power resulted in lower resistivity of the traces. The lowest resistivity was achieved at 40W laser power with a single laser pass. Scanning electron microscopy and energy dispersive spectroscopy were used to characterize the trace morphology and elemental compositions. Higher power laser curing resulted in better bonding of the particles. Laser cured samples had minimal oxidation to the cross-section region of the traces as compared to furnace cured samples. This research lays the foundation for the fabrication of electronic components for a high level of freeform 3D electronics using a hybrid additive manufacturing technology.

Keywords: Additive Manufacturing, Electronics, Laser Curing, Multiphase Material, Sintering Mechanism

Introduction

Electronic devices have a high impact in the industries of automotive, aerospace, healthcare and military. Typically, electronic devices, integrated circuits and printed circuit boards are manufactured using traditional methods (Lopes *et al.*, 2012; Made, 2007). Additive Manufacturing (AM), widely known as 3D printing, can freeform fabricate a 3D object layer-by-layer (Marshall, 2014; Espalin *et al.*, 2014). AM was first introduced in 1987 as Stereolithography (SL) by 3D Systems (Bandyopadhyay and Bose, 2015). The SL process uses a laser on ultraviolet sensitive polymers to solidify the layers of polymer to build 3D structures (Wohlers and Gornet, 2014). Palmer *et al.* (2005) were one of the first to combine direct writing and additive

manufacturing for building robust 3D electronic circuitry. Lopes *et al.* (2012) used hybrid additive manufacturing (SL and direct writing/printing) for embedded electronic circuits using a silver-based ink. Lopes *et al.* (2014) investigated the wavelength of laser curing on conductive ink traces using the 250/50 SL machine. The experiments were performed using two laser wavelengths, several inks and different scanning dynamics to determine the optimal laser curing parameters. The 325 nm wavelength had better volumetric ink curing than the 355 nm, but the 355 nm wavelength has a longer lifecycle. Thus, the research recommended using the 355 nm with post oven curing (Lopes *et al.*, 2014). Roberson *et al.* (2012) used ohmic curing for conductive silver traces. Micro and nanoparticle inks were utilized in the research. With the

ohmic curing method, the conductive trace acted as a heating element. This confined the heat to the area around the conductive trace demonstrating its applicability for a broad range of substrate materials. Ohmic curing is a rapid sintering method conducted at a fraction of the time of oven curing (Allen *et al.*, 2008; Roberson *et al.*, 2012).

AM of conductive traces and PCBs is eco-friendly and produces minimal waste. Another advantage of AM is its ability to make design changes on-the-fly within the CAD file. However, traditional manufacturing methods have limitations of design freedom while building complex shapes.

Hybrid additive manufacturing combines Additive Manufacturing (AM) and two or more manufacturing processes to fabricate a 3D object. Hybrid additive manufacturing has all the advantages of AM in addition to a reduction in setup time (McKenzie *et al.*, 2017). Hybrid additive manufacturing eliminates limitations of the traditional methods (Desai *et al.*, 2013; Parupelli and Desai, 2016). The process allows the deposition of 3D objects without toxic chemicals and masks. It is highly amenable to small production batches. Functional parts/devices can be manufactured in a single setup. Conductive traces are usually thermally cured using a furnace. Prior research has shown that laser curing is possible at a fraction of time over furnace curing (Lopes *et al.*, 2014).

Other curing and sintering mechanisms include microwave (Perelaer *et al.*, 2006) and photonic sintering by a flash lamp (Hwang *et al.*, 2012). The curing of conductive traces has shown a marked reduction in the resistivity of the traces due to the formation of a conductive network pathway. In this research, our group explores the hybrid additive manufacturing process combining microextrusion and picojet deposition methods. In situ laser curing is performed for different process parameters. The sintering mechanism between furnace and laser curing was evaluated based on SEM images and EDS compositional analysis. Laser curing provided comparable resistivity values to furnace curing. This research provides the foundation for fabricating multi-material conductive traces with tunable morphology and composition based on a new hybrid additive manufacturing method.

Materials and Methods

Direct writing/micro-extrusion and PICO-jetting were integrated on a single platform to create a hybrid additive manufacturing system. Micro-extrusion was used for viscous materials (Ready *et al.*, 2013; Yang *et al.*, 2009) whereas, PICO-jetting was used for nanoparticle ink. Micro-extrusion uses a pressurized system to aid the deposition. The PICO-jet uses a piezoelectric actuator for drop-on-demand deposition (Desai and Lovell, 2008, 2009, 2012; Desai *et al.*, 2007; Knowlton *et al.*, 2015; Vaezi *et al.*, 2013). The materials used included carbon, nickel and silver pastes. Nanoparticle silver ink was used for PICO-jetting. The specifications of the pastes and ink are displayed in Table 1. The materials listed in Table 1 were modified for consistent deposition. Water was added to the paste to achieve the ideal viscosity for deposition.
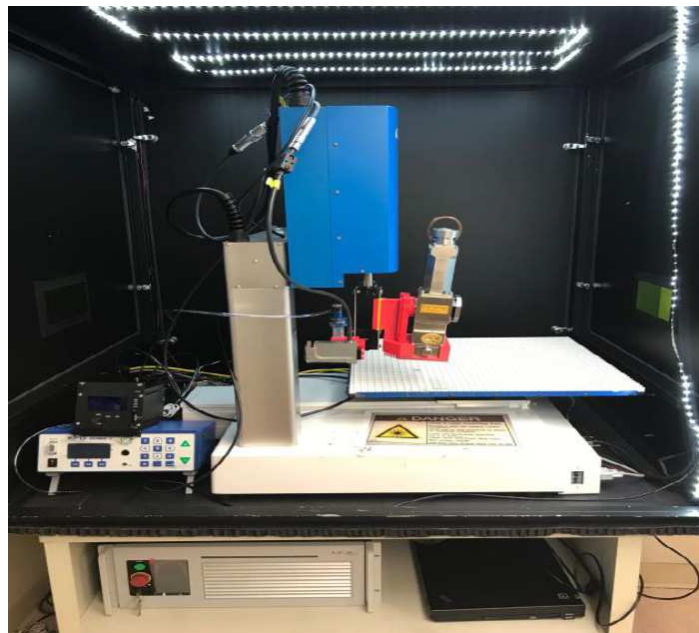

Fig. 1: Hybrid additive manufacturing setup

Table 1: Paste and ink specifications

Ink/paste	Particle size	Particle structure	Ink/ paste color	Initial viscosity	Recommended curing conditions
Carbon	25-100 μm	Flake based	Dark grey	20,000 – 25,000 cP @ 25°C	Air: 2 h. Heat Cure: 2 h. @ 93°C Heat Cure: 2 h. @ 260°C
Silver	20 μm	Flake based	Silver	300,000 – 350,000 cP @ 25°C	Air: 5 min. Heat Cure: 2 h. @ 93°C Heat Cure: 2 h. @ 260°C
Nickel	20 μm	Faked based	Light grey	20,000 – 25,000 cP @ 25°C	Air: 2 to 4 h. Heat Cure: 2 h. @ 93°C Heat Cure: 2 h. @ 260°C
Nanoparticle Silver	53.1 nm	Nano particle	Translucent/Clear	20 – 40 cP @ 25°C	N/A

The fabrication of the materials was conducted using a multi-axis dispensing robot (Nordson EFD desktop JR2200) with a teaching pendant as shown in Fig. 1. The robot uses the x-, y-, z- and R-axis stages for printing the tool path of the traces on the substrate. The PICO-jetting module (PICO xMOD) was attached to the robot head.

Software

A 3D CAD software (SolidWorks®) was used to create different patterns for the conductive traces. Once the CAD model was designed, it was then converted into an "STL" file (Gibson *et al*., 2010). An alternative way to create patterns was to use the teaching pendant of the robot. By using the teaching pendant, patterns were created by assigning coordinate points. The conductive traces were deposited on to the substrates using the CAD software and teaching pendant. ImageJ software (Schneider *et al.*, 2012) was used to measure the cross-sectional area of the traces.

Hardware

A specially designed fixture was used to hold multiple tool heads. These included the microextrusion, laser and PICO xMOD attachments. Syringe barrels were used to extrude the materials on to the substrate. The programmed patterns were deposited onto the substrates based on the x, y and z coordinate points. The micro-extrusion head with a nozzle size of 0.84 mm was used to deposited viscous materials. Micro-extrusion uses pressurized air to aid the deposition of the conductive materials on to the substrates (Perez and Williams, 2013). A pressure system (Ultimus V) was used to control the extrusion of materials. A PICO-jet head (PICO xMOD) was used to deposit less viscous materials. Furnace and laser curing was used to cure the conductive traces. Furnace curing was conducted with the Thermolyne 47900 furnace. In situ laser irradiation was conducted with YLR-series IPG Photonics laser. The spot size of the laser beam was 3mm in diameter

which ensured the encapsulation of the traces for complete curing. Different laser parameters were adjusted which include power, beam size and scanning speed. The laser power ranged from 16 to 40W. A digital multimeter was used to measure the resistance (Keysight Technologies U1282A). Resistivity of the traces was calculated using Equation 1:

$$\rho = \frac{AR}{1} \tag{1}$$

Where:
ρ = Resistivity (kΩ-mm)
A = Cross-sectional area (mm^2)
R = Resistance (kΩ)
l = Length (mm)

An optical microscope (BX51 Olympus) was used to capture the cross-sectional area of the conductive traces. Scanning Electron Microscope (SEM) and Energy-Dispersive X-ray spectroscopy (EDS) (Zeiss Auriga) was used to capture the detailed microstructure and composition. A rheometer (Brookfield DV3T™) was used to measure the viscosity over time.

Results and Discussion

A hybrid additive manufacturing setup using micro-extrusion and PICO-jetting was used to deposit conductive traces with different patterns. Glass slides and flexible Kapton materials were used as substrates. The materials used in the first phase of experimentation included carbon paste, nickel paint and composite paste. The composite paste consisted of carbon, nickel and silver paste homogenously mixed. Each material for the composite paste had an equal weight of 15.5 g. Phase one investigated the optimal curing parameters for both furnace and laser sintering mechanisms. Phase two included the furnace cured samples and phase three was the laser cured samples.

Phase One: Optimal Curing Parameters

The purpose of phase one was to explore the optimal curing parameters with furnace and laser sintering. The materials used were carbon paste, nickel paint, nickel paste and silver paste. A rectangular spiral pattern was designed for carbon traces and the carbon-nickel traces. The carbon-nickel traces had two separate experiments. One experiment had the carbon deposited and the nickel layered on top of the carbon. Both layers were cured simultaneously. The other experiment deposited the carbon and cured it subsequently. Once the carbon was cured, the nickel was deposited and cured. Figure 2 shows examples of the rectangular spiral and serpentine pattern.

The results from the preliminary trails demonstrated that laser curing the carbon and nickel layers simultaneously yielded better results than curing them separately. Different laser parameters were varied to achieve consistent sintering of the deposited materials. The optimal laser curing parameters included a laser z-height of 30 mm and laser line speed of 7 mm/s. These settings were used to cure the composite patterns.

Figure 4 displays the accuracy of the deposition. Figure 4a shows a straight-line pattern of deposition with a width of approximately 1200 μm. Figure 4b shows a blistered spot in the deposited trace due to the localized heating of the material.

Phase Two: Furnace Cured Samples

Phase two demonstrated the furnace curing of the traces and its effect on resistivity. The materials used in the furnace samples were carbon, nickel, silver, composite and carbon-nano silver. For the carbon-nano silver traces, the carbon was first deposited and the nanoparticle silver was PICO-jetted on top of the carbon and cured simultaneously. A straight-line pattern was deposited on glass substrates for a length of 55 mm. The optimal curing parameters for the furnace cured samples are shown in Table 2.

The extrusion pressure was dependent upon the material type and viscosity. Carbon had an extrusion pressure of 2 psi and a viscosity of 34.40cP. Nickel had an extrusion pressure of 3 psi and a viscosity of 19.20cP. Silver had an extrusion pressure of 5 psi and a viscosity of 85.60cP. Composite had an extrusion pressure of 3 psi and a viscosity of 44.00 cP. Carbon-nano silver had an extrusion pressure of 3 psi and a viscosity of 34.40 cP for carbon. The nanoparticle silver ink for the carbon-nano silver traces has a pressure of 1 psi and a cycle time of 9.15 ms with a jetting pulse time of 9.00 ms. The viscosity of the nanoparticle silver ink was very low. Figure 5 shows an example of the cross-sectional measurement using the optical microscope and ImageJ software.

Figure 6 illustrates the resistivity of each material based on furnace curing mechanism. The silver traces had the lowest resistivity with an average of 2.50E-05 kΩ-mm. The composite and nickel had a resistivity of 3.69E-05 kΩ-mm and 1.36E-04 kΩ-mm, respectively. Carbon had the highest resistivity with 5.92E-04 kΩ-mm and the carbon-nano silver had a resistivity of 2.82E-04 kΩ-mm.

Phase Three: Laser Cured Samples

Phase three focused on the laser curing power of the traces and its effect on the resistivity. The materials used were carbon, nickel, silver, composite and carbon-nano silver. For the carbon-nano silver traces, the carbon trace was first deposited and the nanoparticle silver was PICO-jetted on top of the carbon to laser cure simultaneously. A straight-line pattern was deposited on to glass substrates for a length of 55 mm. The extrusion and viscosity measurements were similar to furnace cured samples. Multiple laser curing powers were utilized such as 16W, 25W, 30W and 40W. Table 3 illustrates the optimal curing parameters for the laser.

Figure 7 shows the resistivity values for carbon, carbon-nano silver and composite traces for laser cured samples with a single pass. An increase in the power of the laser resulted in lowering the resistivity values of the traces. The 40W power (highest power setting) had the lowest resistivity values for all the samples. This can be attributed to the enhanced sintering among the particles leading to conductive pathways for the trace.

Figure 8 shows the resistivity values for nickel and silver traces cured using single pass laser. The 40W laser power gave the lowest resistivity values for both nickel (5.29E-05 kΩ-mm) and silver (1.74E-05 kΩ-mm) samples.

Statistical Analysis of Laser Cured Traces

A full factorial design was performed to compare the effects of the resistivity for all materials. The analysis measured the significance of the laser power (n = 4) and material type (n = 5) on the resistivity. The interaction effect of the laser power and material type was also analyzed. The significance level was α = 0.05.

Table 4 shows the ANOVA analysis for the full factorial design. Figure 9 shows that the data was normally distributed and model adequacy check was fulfilled. The ANOVA depicts that all the factors and their interaction are significant. However, the most significant effect was material type with the highest value of F = 1378.10.

655

Morphology Analysis

Scanning electron microscope (SEM) was used to analyze the microstructure of the conductive traces. The furnace trace had few pores and a flaky grain structure. Laser cured samples at 40W power had dense microstructure for the cross-sectional region.

The 40W laser based curing had lower resistivity as compared to furnace cured samples. This can be attributed to better bonding of silver particles forming continuous conductive pathways. Figure 10 illustrates the top view and cross-sectional view SEM images of the furnace and laser cured samples.

Table 2: Furnace curing parameters

Z (mm)	Line speed (mm/s)	Furnace setting	Length (mm)
83	15	2h@93C, 2h@260C	55

Table 3: Laser curing parameters

Z (mm)	Line speed (mm/s)	Laser Z (mm)	Laser line speed (mm/s)	Length (mm)
83	15	30	7	55

Table 4: Minitab ANOVA output (laser power)

Source	DF	Seq SS	Adj SS	Adj MS	F	P
Laser power (A)	3	0.00019	0.00019	0.00060	92.86	0.0001
Material type (B)	4	0.00383	0.00383	0.00900	1378.10	0.0001
A * B	12	0.00018	0.00018	0.00020	21.59	0.0001
Error	40	0.00003	0.00003	0.00001		
Total	59	0.00423				

Table 5: Elemental composition of silver traces

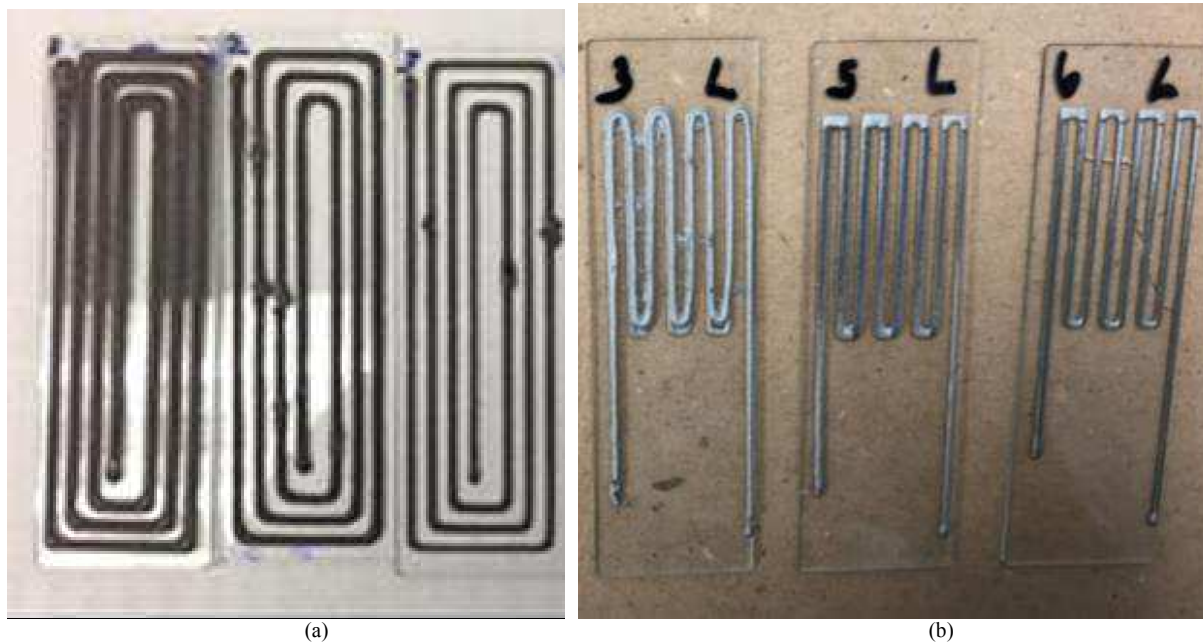| Curing mechanism	Element	Top view weight (%)	Cross-sectional view (%)
Furnace	Ag	40.76	12.18
	O	31.65	55.84
40W laser	Ag	40.79	74.69
	O	26.93	8.99

Fig. 2: (a) Carbon traces (rectangular spiral) (b) composite traces (serpentine)
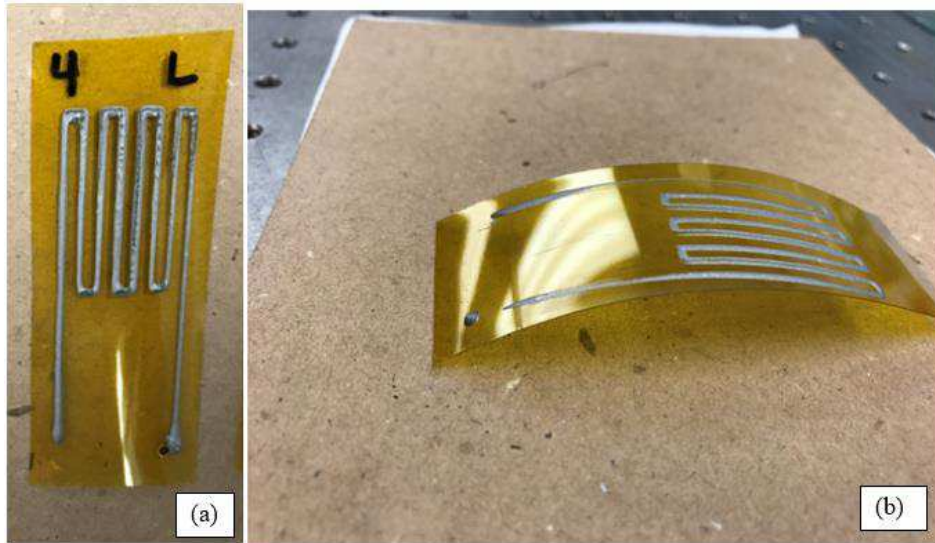
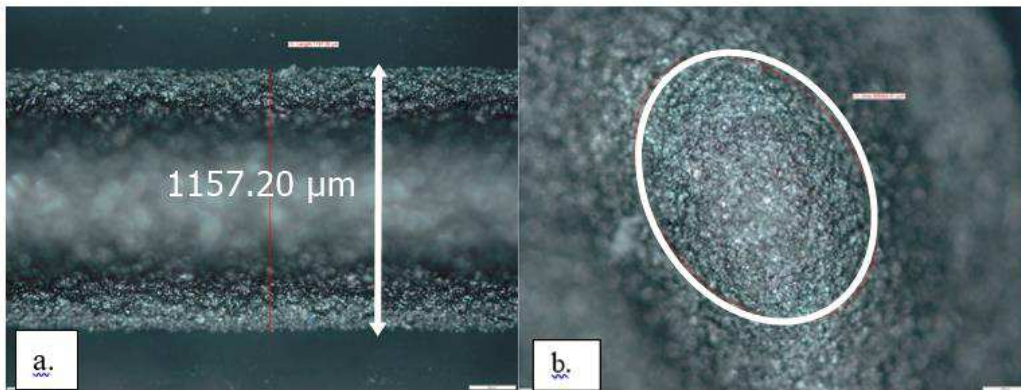**Fig. 3:** Composite paste (serpentine pattern) on flexible Kapton

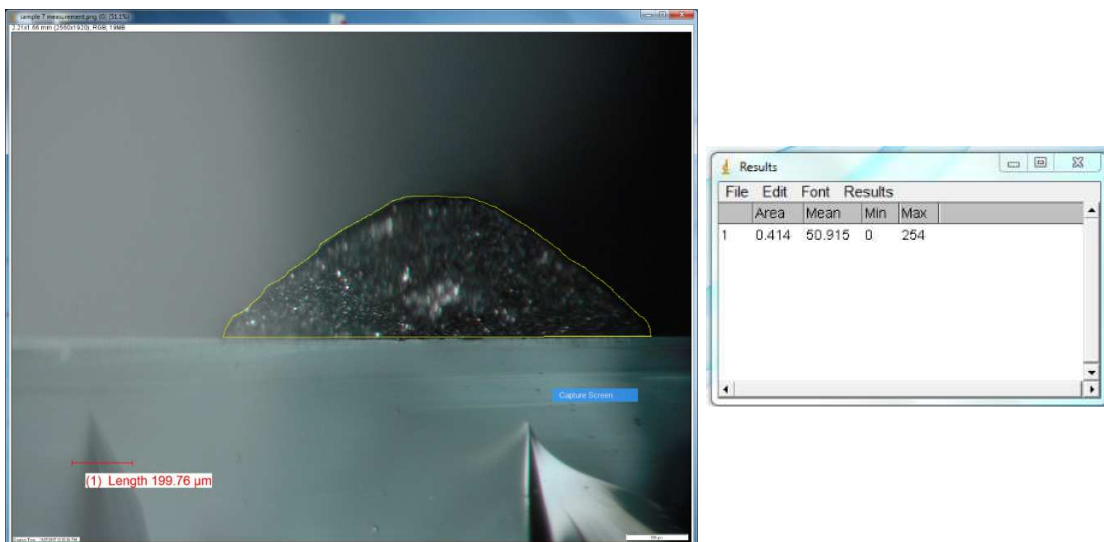**Fig 4:** Optical microscope images of carbon traces in phase one

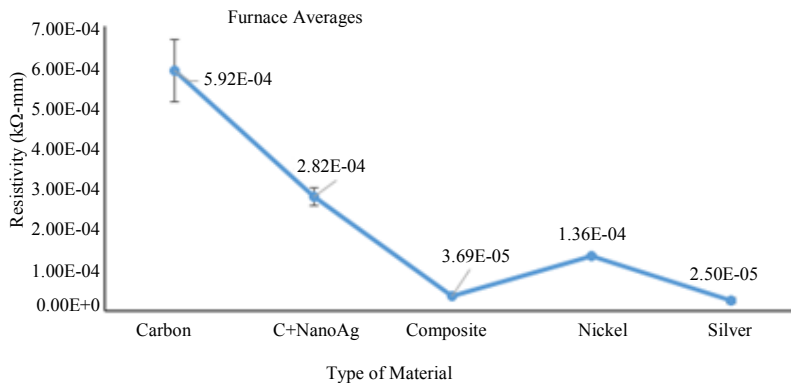**Fig. 5:** Cross-sectional area measurement of carbon traces

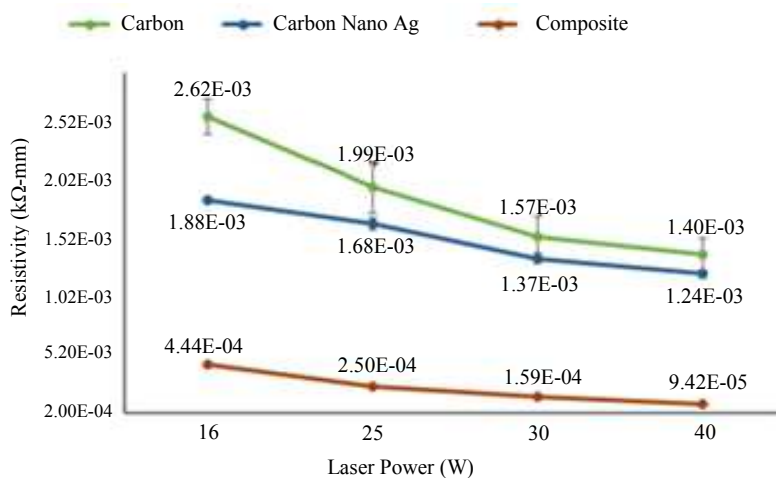**Fig. 6:** Resistivity of furnace cured traces

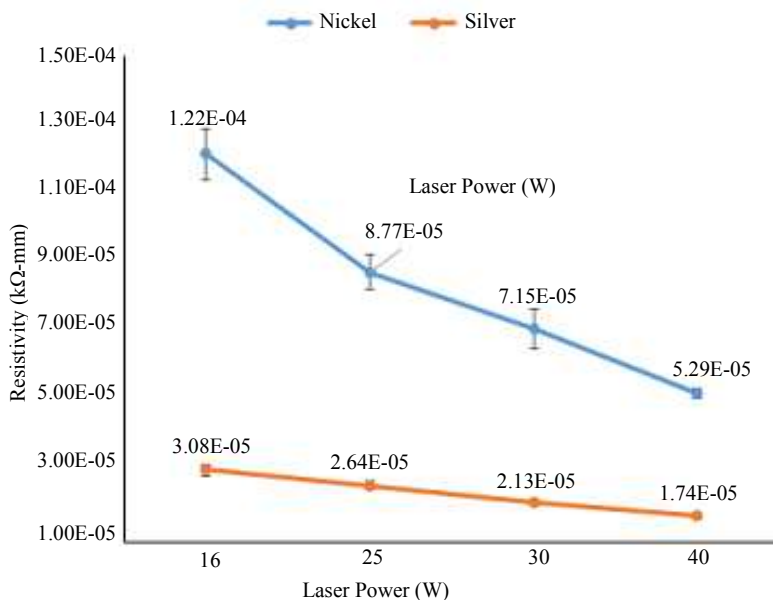**Fig. 7:** Effect of laser power on resistivity of carbon, carbon-nano Ag and composite traces

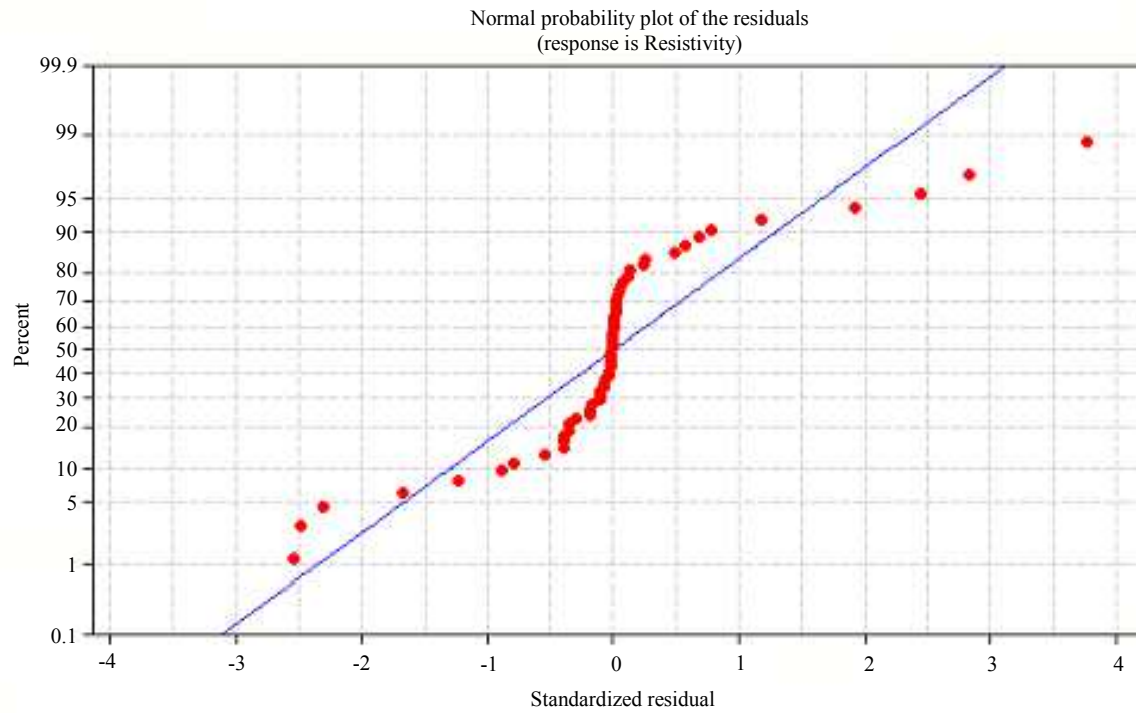**Fig. 8:** Effect of laser power on resistivity of nickel and silver traces

658

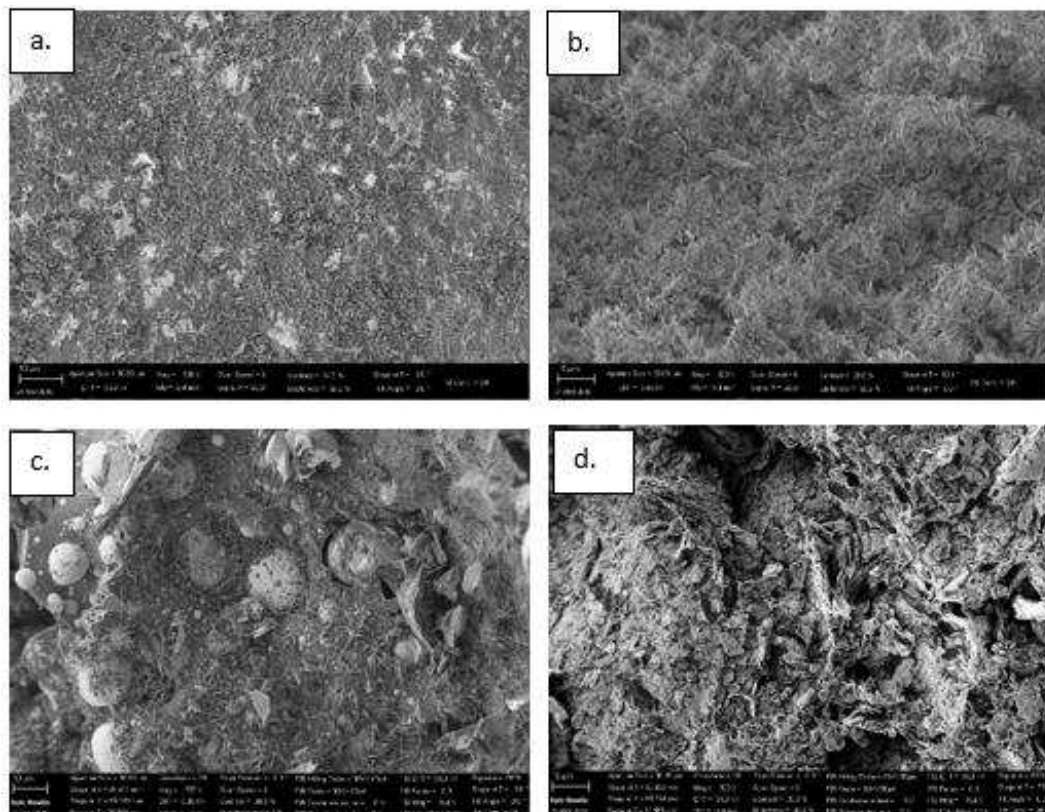**Fig. 9:** Normal probability plot (laser power)

Fig. 10: Cross-sectional SEM images of silver traces (a) furnace top view (b) furnace cross-sectional view (c) 40W laser top view (d) 40W cross-sectional view
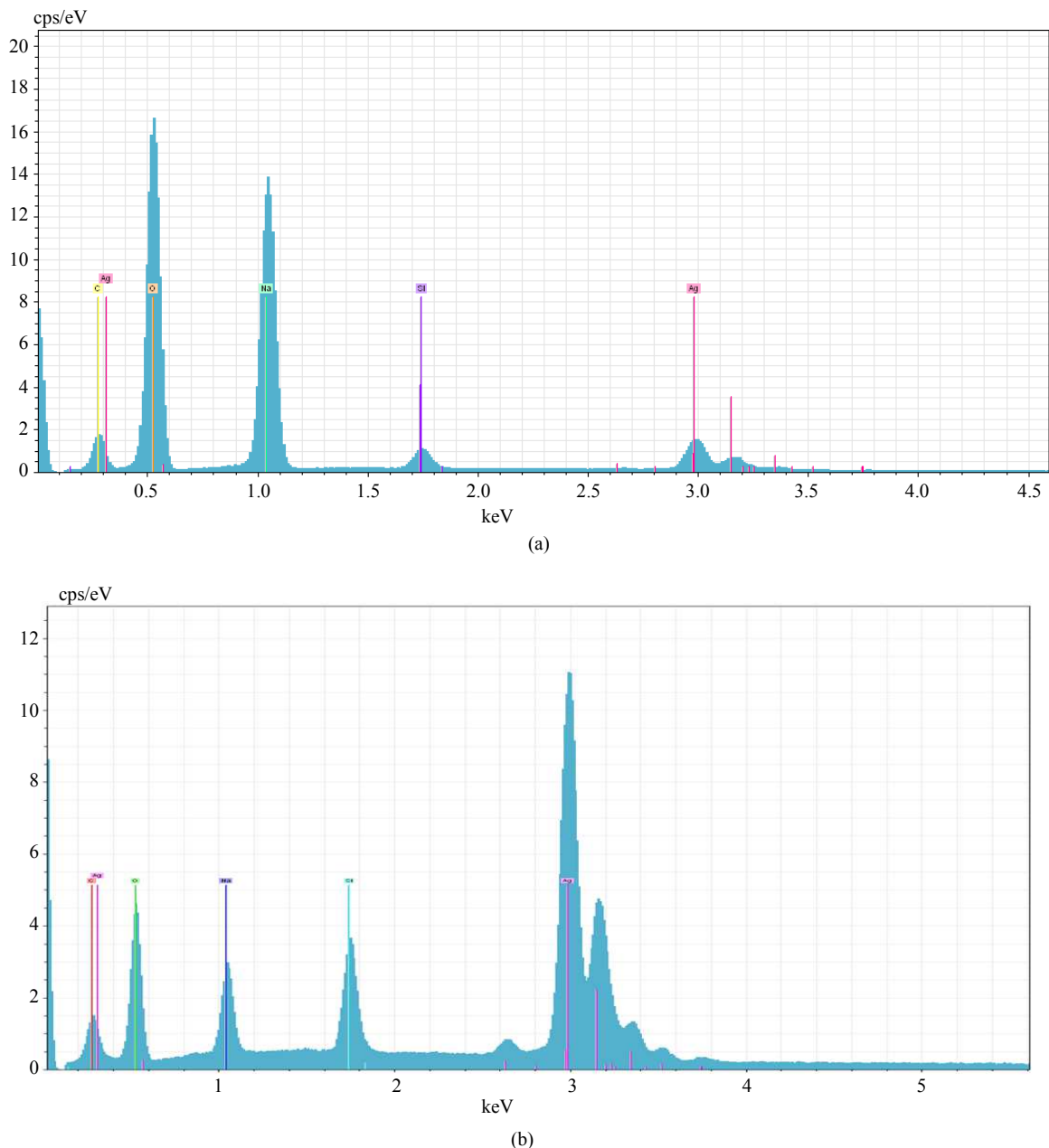
659

(a)

(b)

Fig. 11: EDS of silver trace for (a) Furnace cured (b) 40W Laser

An Energy Dispersive x-ray Spectroscopy (EDS) was conducted for both furnace and laser cured silver traces to determine their elemental compositions Table 5. shows the presence of silver and oxygen as the major constituents in the traces. The presence of oxygen indicates significant surface oxidation in both the traces. The top surface of furnace and laser traces had similar percentages of silver and oxygen content, respectively. However, the cross-sectional region of the furnace sample had substantial oxidation (55.84%) as compared to laser sample (8.99%). This can be

attributed to longer sintering cycles in the furnace cured samples (>2 h.) as compared to laser cured samples (>1 min). Similarly, the presence of elemental silver was significantly higher (74.69%) for the laser sample as compared to the furnace sample (12.18%). These findings correlate with the lower resistivity of 40W laser cured ($1.75e^{-5}$kΩ-mm) samples as compared to furnace cured ($2.5e^{-5}$kΩ-mm) samples.

Figure 11 shows EDS spectra of the elements in both furnace and 40W laser traces. Trace elements such as carbon, silicon and sodium were found in the spectra. An

optical absorption band at ~0.5 keV reveals the presence of silver particles for the furnace cured mechanism (Fig. 11a). Most silver particles were found at ~3 keV optical absorption band for the 40W laser trace (Fig. 11b).

Conclusion

This paper presents hybrid additive manufacturing of multiphase materials using both furnace and laser curing mechanisms. The hybrid additive setup includes micro-extrusion, PICO-jet and laser sintering. The materials used were carbon, nickel and silver paste, nickel paint and nanoparticle silver ink. The materials were deposited on rigid glass and flexible Kapton. Different pattern designs were designed using CAD software and the robot teaching pendant. Phase one of experimentation focused on selecting the optimal parameters for both curing mechanisms. Phase two involved furnace curing of traces and determining the rheological properties of the conductive slurries. In phase three, the laser power was varied for all the traces at 16, 25, 30 and 40W. A decrease in resistivity was observed for all the material compositions with higher laser power. This can be attributed to the better bonding among the slurry particles with increasing laser powers. Carbon-nano silver traces were fabricated by in situ infiltration of nano-silver solution (PICO jetting) within the microextruded carbon trace. The lowest resistivity was observed at 40W laser power where all traces had consistent particle sintering. An important finding of this research was that laser curing had significantly lower oxidation as compared to furnace curing. This is due to the fast laser curing times (< 1 min) as compared to furnace curing (>2 h). The new hybrid additive manufacturing technology developed in this research enables the fabrication of customized electronic components with tunable electrical properties.

Acknowledgement

Funding Information

Author's Contributions

Both the authors conducted statistical and microstructural analysis of the research. All authors contributed to the writing of the manuscript.

Salil Desai: Designed and planned the experiments.
Jasmine McKenzie: Performed laboratory and SEM tasks.

Ethics

The authors declare that there are no ethical issues that could arise after publication of this research study.

References

Allen, M.L., M. Aronniemi, T. Mattila, A. Alastalo and K. Ojanperä *et al*., 2008. Electrical sintering of nanoparticle structures. Nanotechnology, 19: 175-201. DOI: 10.1088/0957-4484/19/17/175201

Marshall, B., 2014. Unlocking the potential of additive manufacturing in the fuel cells industry. Fuel Cell Technologies Office.

Bandyopadhyay, A. and S. Bose, 2015. Additive Manufacturing. 1st Edn., CRC Press. Boca Raton.

Desai, S., M. Craps and T. Esho, 2013. Direct writing of nanomaterials for flexible Thin-Film Transistors (fTFTs). Int. J. Adv. Manufactur. Technol., 64: 537-543. DOI: 10.1007/s00170-012-4425-4

Desai, S. and M. Lovell, 2008. Statistical optimization of process variables in a continuous inkjet process - a case study. Int. J. Industrial Eng. Theory, Applic. Pract., 15: 104-112.

Desai, S. and M. Lovell, 2009. Computational fluid dynamics analysis of a direct write manufacturing process. Int. J. Nanomanufacturing. DOI: 10.1504/IJNM.2009.027424

Desai, S. And M. Lovell, 2012. Modeling fluid–structure interaction in a direct write manufacturing process. J. Mater. Proc. Technol., 212: 2031-2040. DOI: 10.1016/j.jmatprotec.2012.05.006

Desai, S., M. Lovell and J. Cordle, 2007. Coupled field analysis of a piezoelectric bimorph disc in a direct write process. Composit. Part B: Eng., 38: 824-832. DOI: 10.1016/j.compositesb.2006.12.005

Espalin, D., D.W. Muse, E. MacDonald and R.B. Wicker, 2014. 3D Printing multifunctionality: structures with electronics. Int. J. Adv. Manufactur. Technol., 72: 963-978. DOI: 10.1007/s00170-014-5717-7

Hwang, H.J., W.H. Chung and H.S. Kim, 2012. In situ monitoring of flash-light sintering of copper nanoparticle ink for printed electronics. Nanotechnology, 23: 485-205.
DOI: 10.1088/0957-4484/23/48/485205

Gibson, I., W.R. David and S. Brent, 2010. Additive Manufacturing Technologies: Rapid Prototyping to Direct Digital Manufacturing. 1st Edn., Springer, New York, ISBN-10:1441911219, pp: 484.

Knowlton, S., S. Onal, C.H. Yu, J.J. Zhao and S. Tasoglu, 2015. Bioprinting for cancer research. Trends Biotechnol, 33: 504-513.
DOI: 10.1016/j.tibtech.2015.06.007

Lopes, A.J., M. Eric and B.W. Ryan, 2012. Integrating stereolithography and direct print technologies for 3D structural electronics fabrication. Rapid Prototyp. J., 18: 129-143.
DOI: 10.1108/13552541211212113

Lopes, A.J., I.H. Lee, E. MacDonald, R. Quintana and R. Wicker, 2014. Laser curing of silver-based conductive inks for *in situ* 3D structural electronics fabrication in stereolithography. J. Mater. Proc. Technol., 214: 1935-1945.
DOI: 10.1016/j.jmatprotec.2014.04.009

Made, H.P., 2007. Printed circuit board. Made How.

McKenzie, J., S. Parupelli, D. Martin and S. Desai, 2017. Additive manufacturing of multiphase materials for electronics. Proceedings of the IIE Annual Conference Proceedings, (ACP' 17).

Palmer, J.A., J.L. Summers, D.W. Davis, P.L. Gallegos and B.D. Chavez *et al.*, 2005. Realizing 3-d interconnected direct write electronics within smart stereolithography structures. Proceedings of the International Mechanical Engineering Congress and Exposition, Nov. 5-11, Electronic and Photonic Packaging Division, Orlando, Florida, USA, pp: 287-293.
DOI: 10.1115/IMECE2005-79360

Parupelli, S.K. and S. Desai, 2017. Understanding hybrid additive manufacturing of functional devices. Am. J. Eng. Applied Sci., 10: 264-271.
OI: 10.3844/ajeassp.2017.264.271

Perelaer, J., B.J. de Gans and U.S. Schubert, 2006. Ink-jet printing and microwave sintering of conductive silver tracks*. Adv. Mater., 18: 2101-2104.
DOI: 10.1002/adma.200502422

Perez, K.B. and C.B. Williams, 2013. Combining additive manufacturing and direct write for integrated electronics-a review. Proceedings of the 24th International Solid Freeform Fabrication Symposium-An Additive Manufacturing Conference, (AMC' 13).

Ready, S., F. Endicott, G.L. Whiting, T.N. Ng and E.M. Chow *et al.*, 2013). 3D printed electronics. Proceedings of the NIP and Digital Fabrication Conference, (DFC' 13).

Roberson, D.A., R.B. Wicker and E. MacDonald, 2012. Ohmic curing of printed silver conductive traces. J. Electronic Mater., 41: 2553-2566.
DOI: 10.1007/s11664-012-2140-4

Schneider, C.A., W.S. Rasband and K.W. Eliceiri, 2012. NIH Image to ImageJ: 25 years of image analysis. Nature Meth., 9: 671-675.
DOI: 10.1038/nmeth.2089

Vaezi, M., H. Seitz and S. Yang, 2013. A review on 3D micro-additive manufacturing technologies. Int. J. Adv. Manufactur. Technol., 67: 1721-1754.
DOI: 10.1007/s00170-012-4605-2

Wohlers, T. And T. Gornet, 2014. History of additive manufacturing. Retrieved from

Yang, M., Z. Xu, S. Desai, D. Kumar and J. Sankar, 2009. Fabrication of novel single-chamber solid oxide fuel cells towards green technology. Proceedings of the International Mechanical Engineering Congress and Exposition, Nov. 13-19, ASME, Lake Buena Vista, Florida, USA, pp: 61-66.
DOI: 10.1115/IMECE2009-12627